FULL PAPER MANUSCRIPT

Acoustic Phonon Impact on the Inter-Coulombic Decay Process in Charged Quantum Dot Pairs

A. Bande[a]

[a]Institute of Methods for Material Development, Helmholtz-Zentrum Berlin für Materialien und Energie GmbH, Albert-Einstein-Str. 15, 12489 Berlin, Germany

ARTICLE HISTORY
Compiled September 28, 2018

ABSTRACT
Recently, highly-accurate multi-configuration time-dependent Hartree (MCTDH) electron dynamics calculations demonstrated the efficient long-range energy transfer inter-Coulombic decay (ICD) process to happen in charged semiconductor quantum dot (QD) pairs. ICD is initiated by intraband photoexcitation of one of the QDs and leads to electron emission from the other within a duration of about 150 ps. On the same time scale electronically excited states are reported to relax due to the coupling of electrons to acoustic phonons. Likewise, phonons promote ionization. Here, the QDs' acoustic breathing mode is implemented in a frozen-phonon approach. A detailed comparison of the phonon effects on electron relaxation and emission as well as on the full ICD process is presented, which supports the previous empirical finding of ICD being the dominant decay channel in paired QDs. In addition the relative importance of phonon-phonon, phonon-electron, and electron-electron interaction is analysed.

KEYWORDS
Quantum dots; electron dynamics; inter-Coulombic decay; resonance states; phonons

1. Introduction

Phonons are associated with temperature-induced quasi-particle collective normal-mode vibrations of several, even a large number, of atoms in the crystal lattice of a solid state material. They couple effectively to electrons and therefore have a strong impact on properties and processes in condensed matter. Reported occurrences range from temperature effects on optical spectra [1–3] and band structures [4–7] over the decay of plasmonic states [8] to hot carrier relaxations [9–11] in various extended metal and semiconductor structures.

Also in nanostructured materials, e.g. in semiconductor quantum dots (QDs), numerous electron-phonon scattering effects have been reported that modify the excitation [12, 13] or relaxation [14–19] properties of thermally or optically excited electronic states, i.e. intraband excitations or excitons. Last but not least they affect the electrons' interaction with the QD's environment through modified tunneling [20, 21] as well as electron capture [22–27] and emission behavior [25].

CONTACT A. Bande. Email: annika.bande@helmholtz-berlin.de

QDs have nowadays developed into state-of-art semiconductor heterostructure materials implemented into many top-modern devices as for instance QD lasers [28, 29], LEDs [29, 30], transistors [31], detectors [32], or solar cells [33, 34]. Moreover, their role in biomedical applications [34], catalysis [34] and particularly energy conversion [33, 35], as well as in the field of quantum information processing [36–38] is constantly growing and further applications are to come. Hence, a deep insight into the QDs' fundamental working principles including the aforementioned phonon mechanisms is critical. For example in QD lasers, charge-carrier recombination under photon emission sensitively depends on the phonon-mediated electron and hole trapping [39]. Particularly a detailed knowledge of characteristic time scales is of utter importance for any discovery of novel processes in composite QD materials.

Although not the only ones, significant contributions towards the understanding of electron-phonon interactions in QD processes are being made by theoretical ab initio methods. Phonons themselves can be obtained for geometry optimized QD structure with up to 1000 atoms as vibrational eigenfunctions and are the most accurate possible representations of lattice vibrations [40]. However, from such calculations no insight on how phonons manipulate the electronic properties can be gained.

For the electronic structure a quantum-mechanical representation of the electrons is needed [41–44]. As one option all atoms in the specific QD geometry are calculated explicitly in a discrete [45] or periodic formulation [46–48] of a large-scale electronic-structure approach as e.g. density-functional theory (DFT) in due consideration of the size of the QD. This results in a comprehensive representation of the rich electronic structure of a QD including possible defects or surface states, but describes the electron-electron correlation only insufficiently, as only in cases a configuration interaction description is achievable [49] in a fully-atomistic QD.

At the cost of sacrificing detailed knowledge on the QD's geometry in approximating it by an electron binding potential within the effective mass approximation (EMA) [50], this shorting can be overcome by the usage of correlated methods, as e.g. configuration interaction [51, 52] or multireference perturbation theory approaches [53]. The EMA is moreover known to be a decent approach for QDs larger than 1.5 nm [54] giving single-electron levels in the quality of DFT tight-binding calculations [55–58]. Balancing among both approaches for accurate single- or many-electron properties is necessary. The important electron-phonon interaction can in principle be included within both frameworks, itself at different levels of integrity.

For a combined view on electrons and phonons, the highest possible level is a quantum-mechanical representation of on the one hand the phonon-term itself and on the other hand the electron-phonon coupling within the so-called system-bath approach [49, 59–63]. The charge carriers in the model system are coupled here to a bath of quantum harmonic-oscillator degrees of freedom representing the phonons. Alternatively, analytical expressions for each of the phonon terms can be derived for then calculating dissipation rates from Fermi's golden rule [64] or in the framework of density-functional perturbation theory [65], to name a few.

Independent of the method distinctions are made among the three most common coupling mechanisms of phonons with charge carriers [64]. The Fröhlich interaction accounts for optical phonons which establish polarons in the crystal lattice. Hence, a dipole-dipole coupling term is assumed similarly to that of optical fields. Per contra, acoustic phonons induce deformations of the material and give rise to a deformation and a piezoelectric term, of which the first is known to be more significant on average [64].

Based on the idea of the Born-Oppenheimer approximation, phonons can, however,

be treated classically. In the respective frozen-phonon approach, the nuclear vibration periodically distorts the crystal lattice of the solid, and thus also its electronic structure and with that drives the electron dynamics [66, 67]. Implicitly this means that no actual electron-phonon coupling term is defined and its expectation value quantified, but comparisons are being made for the phonon-free system and for snapshots or the full time-dependency of oscillatory nuclear motion [66]. An example was found in fully-atomistic calculations [68]. In this work I adapt the idea of the frozen-phonon approach for the time-dependent modification of the QD binding potential and revisit the inter-Coulombic decay (ICD) process in paired QDs (PQDs), for which to present only empirical estimates were given [69].

ICD is an ultrafast energy transfer processes mediated by long-range Coulomb interaction that has been discovered in the 1990ties [70]. It is nowadays widely known in atomic and molecular cluster physics [71, 72], but basically understood to potentially appear in many more fields as e.g. biophysics [73–76] or nanoscience [77–79]. In any case an excited electron in one of the subsystems (atom, molecule, molecular fragment, nanoparticle, QD, etc. [72]) decays efficiently to a lower energy or even into its ground state while another electron is emitted from one of the neighboring subsystems.

In a series of papers on pairs of singly-charged QDs, we particularly elucidated the electron dynamics of ICD [69, 80–84] with highly-accurate MCTDHF-like calculations [85, 86] (multiconfiguration time-dependent Hartree-Fock). Motivation for this attempt has always been the curiosity in the time development of the electronic situation which cannot be addressed neither by non-Hermitian electronic structure theory for resonances [87–90] nor by nuclear dynamics of the cluster explosion after ICD [91–93] otherwise used in the prediction of ICD rates. The latter studies, however, brought forth that motion of nuclei has significant impact on ICD, hence in QD-ICD lattice vibrations should as well.

Our previous empirical argumentation on the charged PQDs was along the lines of the considered electronic energy differences for the envisaged decay being in the range of meV (5.9 meV in the case of GaAs) [80], hence ruling out any effects of optical vibrational modes (36 meV in GaAs [94, 95]) as they would require an exact matching of energies for efficient coupling [16]. Regarding acoustic phonons the argumentation was that an excited state decay mediated by phonons being in the range of sub-nanoseconds [14] is expectedly slower than ICD with a decay time of about 150 ps [69].

However, we are aware that in a specific scenario, the two time-scales may come to a matching and hence phonon-effects might be strongly competitive to ICD. Further, acoustic phonons may as well influence the emission of the ICD electron, which has not been discussed before. Phonon-mediated electron emission in InGaAs/GaAs QDs was for example reported to be in the range of 100 ps [96]. Hence, in order to give a solid proof on the competitiveness of ICD, I implement phonons into the approved methodology as time-dependent modifications of the EMA confinement potentials in the framework of our electron dynamics theory. This is in the spirit of how in attosecond science atomic binding potentials are periodically modified under irradiation of an external electric field [97]. Transferring this strategy to QDs means modelling the acoustic phonons' macroscopic deformation effects on QDs, namely torsional, elongation, and breathing modes [54].

In establishing the relevant operators I am in place to investigate various aspects of phonons as their spatial direction, frequency and oscillation amplitude dependence, as well as interaction effects of phonons on both QDs with each other and their interaction with each of the electrons in either one of the QDs. To do so I at first briefly review

the present mathematical state of the electron dynamics calculations in binding model potentials (Sec. 2.1). In Sec. 2.2 I present the basic physical properties of acoustic phonons and lay out my implementation. Then the computational details are given in Sec. 3. For analysing phonon effects I start with investigating single one-electron QDs in Sec. 4.1 for decay and emission, move on to single-electron PQDs (Sec. 4.2), and finally to the full picture of two-electron PQDs (Sec. 4.3). In a discussion (Sec. 5) additional viewing angles on optical phonons, time scales, and related processes are offered and I conclude (Sec. 6) a first quantitative estimate to acoustic phonon effects on ICD.

2. Theory

2.1. Electron Dynamics in Quantum Dot Binding Potentials

The prediction of electronic processes in QDs using a high-accuracy description of the electron dynamics goes hand in hand with applying the general EMA binding potential representation of the QDs [50]. The respective unperturbed electronic Hamilton operator $\hat{H}^0(\mathbf{r}_1 \dots \mathbf{r}_n)$ for n electrons in m QDs reads

$$\hat{H}^0(\mathbf{r}_1 \dots \mathbf{r}_n) = -0.5 \sum_{i=1}^{n} \nabla_i^2 - \sum_{i=1}^{n} \sum_{k=1}^{m} V_k^{conf}(\mathbf{r}_i) + \sum_{i=1}^{n} \sum_{j>i}^{n} r_{ij}^{-2} \tag{1}$$

with the kinetic energy operator for each electron i in the first and the Coulomb interaction operator for electrons i and j in the last term. V_k^{conf} are the QD confinement potential operators. To be most general the Hamiltonian of Eq. (1) is represented in scaled atomic units, meaning that an electron has the mass $m = 1$ a.u. and the dielectric constant for any material is set to vacuum conditions, i.e. $\kappa = 1$ a.u.

The specific QD material, GaAs in this work, has the effective mass $m^* = 0.063$ and the dielectric constant $\kappa = 12.9$ [94]. The effective mass conversion [50] is hence used to switch from experimental QD sizes L^{QD} in atomic units to lengths L in scaled atomic units [77, 80, 98] used in the calculation according to

$$L^{QD} = L \; a_0 \frac{\kappa}{m^*} \tag{2}$$

where a_0 is the Bohr radius. Likewise energies and times are converted with

$$E^{QD} = E \; \frac{m^*}{\kappa^2} \text{ and } \; t^{QD} = t \; \frac{\kappa^2}{m^*}. \tag{3}$$

For readability the GaAs QDs quantities L^{QD} etc. are in the following given in SI units.

The confinement $V_k^{conf}(\mathbf{r}_i)$ are selected so that they match the experimentally known electronic structures of QDs' conduction bands of a given material composition and shape [41, 99] as well as the physics of the system. Common model representations are square-well potentials [100] or parabolic wells [101, 102] and for ionizable QDs Gaussian or finite square potentials whose widths directly connect to the shapes of the QDs [103]. The depths of the binding potentials are geometry dependent and connected to the relative conduction band onsets of the considered QD and neighboring

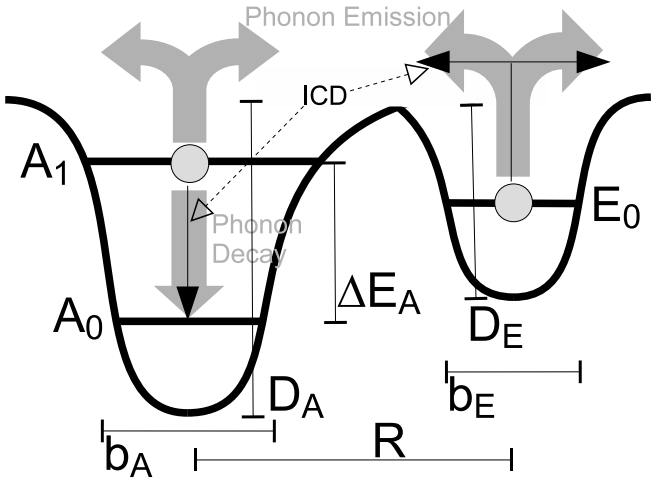

Figure 1. Schematic representation of the two-electron PQD including the geometric measures of Eq. (4). The thin black arrows sketch the ICD process. The thick gray downwards arrow indicates phonon-mediated decay, both grey upwards arrows phonon-mediated emission.

material and with that also to band gaps or electronic excitation energies.

The specific model for the paired QDs (PQDs) [69, 80–83, 104] is

$$V^{conf}(\mathbf{r}_1 \dots \mathbf{r}_n) = 0.5 \sum_{i=1}^{n} \omega_\perp^2 (x_i^2 + y_i^2) - \sum_{i=1}^{n} \sum_{k=1}^{m} D_k e^{-b_k (z_k - z_i)^2}, \tag{4}$$

composed of an harmonic oscillator confinement potential in x and y direction and $m = 2$ inverse Gaussian potentials in the z direction (cf. Fig. 1). It is quasi one-dimensional in the sense that levels in the z direction with energies above D_k are continuum levels of unconfined electrons.

The electronic energies as well as real eigenfunctions of the system can be determined from the time-independent Schrödinger equation

$$\hat{H}^0(\mathbf{r}_1 \dots \mathbf{r}_n)\Phi_a(\mathbf{r}_1 \dots \mathbf{r}_n) = E_a \Phi_a(\mathbf{r}_1 \dots \mathbf{r}_n) \tag{5}$$

when being evaluated on a finite grid.

The electronic boundary condition for ICD in a PQD is that the light-accepting QD (AQD) shown on the left side in Fig. 1 has at least two electronic levels that are termed A_0 and A_1 according to their energetic order. The electron emitter QD (EQD) needs one level E_0 energetically located in between the other levels such that the energy condition

$$\Delta E_A = E_{A_1} - E_{A_0} \geq E_T - E_{E_0} = \Delta E_E \tag{6}$$

with E_T being the ionization threshold is fulfilled.

Several same-spin two-electron states can be accommodated in such a PQD system [80]. The lowest-energy one is the bound A_0E_0 state with one electron in the acceptor and one in the emitter QD. The next higher is a shape resonance state A_0A_1 with both electrons located in the AQD on different levels. Finally, the highest-excited localized state A_1E_0 with one electron in each dot is the metastable Feshbach resonance that

decays via the interatomic Coulombic decay process into a final continuum state with one electron having decayed to the A_0 level of the AQD and the EQD electron having been ionized [80].

Electron dynamics calculations of ICD use a real state function $\Phi_a(\mathbf{r}_1 \dots \mathbf{r}_n)$ from Eq. (5) as initial wave function $\Psi(\mathbf{r}_1 \dots \mathbf{r}_n, t = 0)$ for solving the complex time-dependent Schrödinger equation

$$i\frac{\partial\Psi(\mathbf{r}_1 \dots \mathbf{r}_n, t)}{\partial t} = \left(\hat{H}^0(\mathbf{r}_1 \dots \mathbf{r}_n) - iW_z^L - iW_z^R\right)\Psi(\mathbf{r}_1 \dots \mathbf{r}_n, t), \tag{7}$$

which contains besides the unperturbed Hamiltonian of Eq. (1) two complex absorbing potentials (CAPs) of the form

$$W_z^{L/R} = \eta|z - z_0^{L/R}|^n\,\Theta(z - z_0^{L/R}). \tag{8}$$

They are located on the left (L) or right (R) side of the PQD model potential on the z coordinate and hinder backscattering of the emitted ICD electron from the boundaries of the grid on which I perform the calculations. For this reason their order n, onset $z_0^{L/R}$ located through Heaviside step functions $\Theta(z - z_0^{L/R})$, and strength η are optimized for complete, but non-disturbing removal of the ICD electron at the kinetic energy.

2.2. Time-Dependent Implementation of Acoustic Phonons

Phonons are vibrations of the crystal lattice of a solid which, as any nuclear motion in general, affect the electronic structure and electron dynamics. Two types of phonons can be distinguished with respect to the underlying vibration and interaction patterns.

For completeness, one type of them are the optical phonons which are vibrations of individual atoms against each other. They induce a dipole moment coupling to electronic transitions. The dipole-dipole coupling bears a resonance constraint, i.e. level spacings need to match the phonon energy. In bulk semiconductor materials this is fulfilled whenever the phonon energy exceeds the band gap energy because of the electronic continuum of the bands. The spatial limitation of QDs encloses as peculiarity the so-called phonon bottleneck [64], a quantum effect trivially know from molecular systems. Discretization of energy spacings in finite-size materials counteracts exact fulfillment of the resonance condition and hence fostering of relaxation by optical phonons. This is the case here where the optical phonon frequency of 36 meV [94, 95] exceeds $\Delta E_A = 5.9$ meV.

Different is the situation of the second type of phonons, the acoustic phonons in the energy range of few meV. A view on the mechanism reveals that, similar to what is observed in molecular far-infrared spectroscopy, complete volume elements, i.e. several units cells of the crystal lattice, are set into a concerted vibration into the same direction. In a QD this may lead to a macroscopic effect, e.g. to a breathing, an elongation, or a torsional deformation [54]. The underlying electron-phonon interaction is hence termed deformation type which figuratively means that the deformation of the QD induces a shift of electronic energy levels. The electronic eigenfunctions of the non-vibrating QD are no eigenfunctions to any deformed QD and are, upon vibration, leaking out of the QD into other bound or continuum states. This so-called dissipation can lead to excited state relaxation or ionization.

In the present description the deformation can be achieved by making the potentials

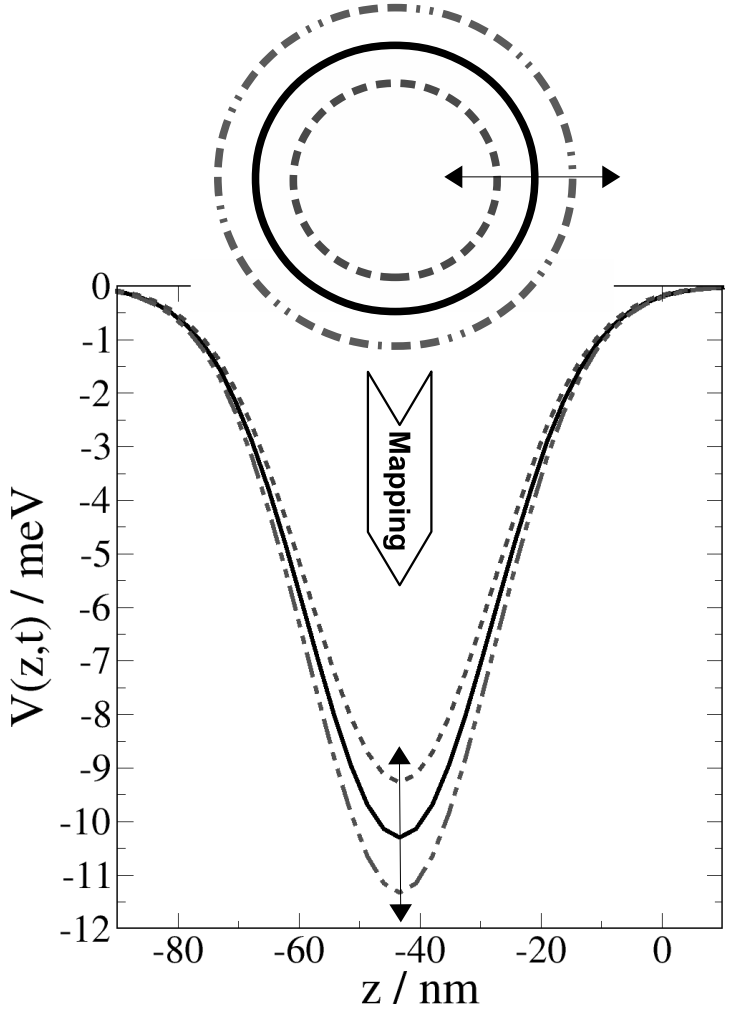

Figure 2. Variation of the acceptor quantum dot binding potential $V(z,t)$ in z direction with relative displacements $\Delta r/r = 0.02$ at times $t = 0$, π, and 2π (solid line), $t = 0.5\pi$ (dashed line) and $t = 1.5\pi$ (dashed-dotted line).

time-dependent as $V(\mathbf{r}) \to V(\mathbf{r},t) = V(\mathbf{r}) + V(t)$. In setting up the matrix formulation for a two-state system,

$$\begin{pmatrix} T(\mathbf{r}) + V(\mathbf{r}) + V(t) & 0 \\ 0 & T(\mathbf{r}) + V(\mathbf{r}) + V(t) \end{pmatrix} \begin{pmatrix} |A_0\rangle \\ |A_1\rangle \end{pmatrix}, \tag{9}$$

it becomes apparent that $V(t)$ is on the diagonal. Therefore, strictly speaking, it is no coupling operator for the electronic ground and excited states. Hence it will not exclusively lead to a $|A_1\rangle \to |A_0\rangle$ relaxation, but is expected to dissipate A_1 into all states including the ionized ones.

The phonon-free potential of Eq. (4) is separable with respect to the three spatial dimensions, i. e. $V(\mathbf{r}) = V(x) + V(y) + V(z)$. Hence each of them is individually to be brought into a phonon-containing form as $V(z) \to V(z,t)$ etc. In assuming that phonons are harmonic vibrations, I incorporate them as periodic oscillators of each of the existing binding potentials. A picturesque representation of this ansatz can be found in Fig. 2 where it is shown how the breathing mode of a QD is translated into

the breathing of an inverse Gaussian model potential. A corresponding mathematical formulation is

$$V(z,t) = -D_k e^{-b_k z^2} \left(1 - \frac{\Delta r}{r} \sin(\omega_{Phon} t)\right). \tag{10}$$

In this equation ω_{Phon} is the frequency of the acoustic phonon and $\Delta r/r$ the amplitude of the vibration with the interpretations of the maximal atom displacement. Note that in Eq. (10) phonons lead to potential depth variation which stands for a material change by either doping or by distortion of the elementary cell. Another possible and equally meaningful implementation is a periodic change of b_k reflecting the QDs' heights [81, 83]. For the harmonic oscillator confinement potentials in the x and y direction the targeted oscillation of the energetic level landscape is realized by

$$V(x,t) = 0.5\, \omega_\perp^2 x^2 \left(1 - \frac{\Delta r}{r} \sin(\omega_{Phon} t)\right). \tag{11}$$

It can be rationalized as a width variation of the harmonic oscillator through $\omega_\perp$ which connects directly to the width of the explicit QD material [81].

In both equations (10) and (11) the parameters ω_{Phon} and $\Delta r/r$ appear. ω_{Phon} is empirically available as database value from experimental infrared spectra on bulk semiconductors at the Γ point of the crystallographic reciprocal grid, where for direct semiconductors as GaAs the direct band gap is located [94, 95, 105]. Instead the maximal displacements $\Delta r/r$ are no physical observables which is why no reference data is available. Therefore a scan through a range of displacements supported by rationalization of myself and of others will deliver an interpretation of its effect on the phonon decay rate.

3. Computational Details

Calculations are performed with the MCTDHF method with the triplet-state's antisymmetry-constraint $A_{ij} = -A_{ji}$ for the reason that the wave function

$$\Psi(\mathbf{r}_1, \mathbf{r}_2, t) = \sum_i \sum_j A_{ij}(t) \varphi_i(\mathbf{r}_1, t) \varphi_j(\mathbf{r}_2, t), \tag{12}$$

is most flexible because both, the single-particle functions (SPFs) φ_i and the expansion coefficients A_{ij} are propagated in time. Therefore a most accurate description of localized bound and excited state functions and delocalized continuum functions and of the electron correlation is likewise possible.

The initial wave function of the resonance state A_1E_0 is obtained from a block relaxation calculation [106]. It is picked from a set of 52 triplet eigenstates $\Phi_n(\mathbf{r}_1, \mathbf{r}_2)$ by inspecting the electron density on the z coordinate of one of the electrons integrated over all degrees of freedom. In the real-time propagation, for which the equations of motion were obtained by applying the Dirac-Frenkel variational principle to the TDSE (Eq. (7)), the integrator accuracy 10^{-7} a.u. (about 10^{-6} meV) and $i = j = 8$ SPFs are used. The autocorrelation function among the initial and time-dependent wavefunction is calculated for analysis. The exponential decay of its squared absolute value allows to finally determine the ICD and phonon decay rates.

To solve the TDSE with the Heidelberg MCTDH program [106, 107] the operators need to be defined on a grid. For the PQD potential of Eq. (4), or either one of the acceptor or the emitter QDs, the parameters have been adapted from previous works [81] to allow for the best track record of changes induced by the phonons. The Gaussian wells depths are $D_A = 10.30$ meV (1.0 a.u.) and $D_E = 8.24$ meV (0.8 a.u.). The AQD and EQD heights of 36.08 and 18.04 nm are deduced from the widths parameters $b_A = 0.25$ a.u. and $b_E = 1.0$ a.u. The QDs are separated by $R = 86.68$ nm (8.0 a.u.) and finally the width of both QDs is determined by $\omega_\perp = 1.0$ a.u. which corresponds to a diameter of $2r_\perp = 28.84$ nm.

The Coulomb operator enters in a regularized form [80]

$$r_{12}^{-1} \Rightarrow [r_{12}^2 + 0.1^2 \cdot e^{-100 r_{12}}]^{-1/2}, \tag{13}$$

to avoid the singularity at the coalescence point of both electrons. During the POTFIT algorithm of MCTDH [107–109], where it is brought into a sum-of-products form, it is further cut at energy $v_{cut} = 10.30$ meV (1.0 a.u.) [81].

The grid in the x and y direction is spanned by five harmonic oscillator DVR grid points (DVR = discrete variable representation) and in the z direction by 185 sine DVR points on a length from $-L = -524$ nm to $+L = +524$ nm (50 a.u.). The CAP operators (Eq. (7) and Eq. (8)) set on at $z_0^L = -325$ nm and $z_0^R = +325$ nm (30 a.u.) and range until the grid's ends. They are of order $n = 4$ and strength $\eta = 8.68 \cdot 10^6$.

Acoustic phonons are finally implemented according to the Eqs. (10) and (11). Each equation requires a phonon frequency from a standard database for GaAs [94, 95]. I use the frequency of transversal acoustic phonons at the X point $\omega_{phon}^{GaAs} = 17.5$ meV ($\omega_{phon} = 1.47$ a.u.). No value at the Γ point exists, but typically values at these two reciprocal lattice points are in fair agreement [105]. For the size variations $\Delta r/r$ no reference values exist. At the same time its choice will affect the shape of the binding potential extremely strongly, so that e.g. the Gaussian potential may lead to the shift of the A_1 state into the continuum at values of about $D_A(1 - \Delta r/r) = 0.5$ or even periodically disappear completely if $\Delta r/r$ was set to 1.0. I probe phonon dissipation rates for both electrons separately and together on the range $0.001 \leq \Delta r/r \leq 0.5$ and give a clear rationalization for the final choice of $\Delta r/r$ leading to a few exemplary values.

4. Results

4.1. One-Electron Single Quantum Dot

4.1.1. Phonon-Mediated A_1 Dissipation

In the AQD with two levels phonon-mediated dissipation (decay, tunnelling, emission, grey arrows on the AQD in Fig. 1) is possible and may be competitive to simple radiative $A_1 \rightarrow A_0$ decay. To investigate this, I add to the AQD of Eq. (4) time-dependent binding potentials (Eqs. (10) and (11)) and run the electron dynamics from the initial state A_1. Several unknowns are benchmarked in the following, namely the displacement parameter $\Delta r/r$, the spatial coordinate for phonons, and the vibration's onset time.

The range of values scanned for Eq. (10) is $0.001 \leq \Delta r/r \leq 0.5$. It was chosen according to a simple rationalization. In case of the approximate average QD radius

Table 1. Acoustic phonon A_1 dissipation rate Γ^{A1}_{1p1e} in meV as function of the displacement parameter $\Delta r/r$.

$\Delta r/r$	Γ^{A1}_{1e1p}/meV
0.001	$2.10{\cdot}10^{-7}$
0.002	$8.37{\cdot}10^{-7}$
0.005	$5.23{\cdot}10^{-6}$
0.008	$1.34{\cdot}10^{-5}$
0.010	$2.09{\cdot}10^{-5}$
0.020	$8.36{\cdot}10^{-5}$
0.050	$5.22{\cdot}10^{-4}$
0.080	$1.34{\cdot}10^{-3}$
0.100	$2.09{\cdot}10^{-3}$
0.200	$8.30{\cdot}10^{-3}$
0.300	$1.87{\cdot}10^{-2}$
0.400	$3.32{\cdot}10^{-2}$
0.500	$5.10{\cdot}10^{-2}$

of $r = 15$ nm considered here, the largest investigated $\Delta r/r = 0.5$ would lead to an absolute displacement of $\Delta r = 7.5$ nm which would mean that the full QD would experience a growth of 50 % within the breathing mode. It further signifies that the outermost atoms of the QD will be displaced by 7.5 nm which is approximately 20 times the nearest neighbour distance in the solid semiconductor material. Such a growth seems impossible, particularly when solid or liquid media is surrounding the QD as e.g. in self-assembled or colloidal QDs, respectively. Lower absolute displacements from $\Delta r = 0.3$ nm ($\Delta r/r = 0.02$) down to $\Delta r = 0.075$ nm ($\Delta r/r = 0.005$) are more reasonable as they are in the order of bond distances. Actually $\Delta r/r = 0.01$ is a value commonly used in the literature [110], and also the smaller $\Delta r/r = 0.001$ has been mentioned [111]. And indeed a QD size variation $\Delta r/r = 0.001$ ($\Delta r = 0.015$ nm), i.e. by only a tenth of a bond length, is at the lower edge of reasonable displacements $\Delta r/r$, because they are barely having an effect on the collective breathing of the QD.

As result of the scan for the dissipation of the A_1 initial state by z-directed acoustic phonons the respective single-electron single-QD dissipation rates Γ^{A1}_{1e1p} are plotted as function of their relative displacements $\Delta r/r$ in Fig. 3 (straight line), numeric data is collected in Tab. 1. From the visualization I deduce a strong rate increase with increasing $\Delta r/r$. From $\Delta r/r = 0.08$ Γ^{A1}_{1e1p} exceeds the radiative decay rate of $\Gamma^{RD} = 1.15 \cdot 10^{-4}$ meV ($1.12 \cdot 10^{-5}$ a.u.) reported in previous works [80]. From $\Delta r/r = 0.2$ it also exceeds the ICD rate $\Gamma^{ICD}_{2e2p} = 4.13{\cdot}10^{-3}$ meV ($4.01{\cdot}10^{-4}$ a.u.) calculated in Sec. 4.3.1 in full agreement with former works. Hence, throughout this study I assume a displacements of $\Delta r/r = 0.02$ as one of the larger values from the rationalization above. With that the phonon-mediated dissipation rate is at most $\Gamma^{A1}_{1e1p} = 8.36 \cdot 10^{-5}$ meV which means two orders of magnitude smaller than that of the ICD rate.

In the underlying A_1 dissipation model bringing the A_1 electron into the A_0 or continuum levels is an effect in the z coordinate of the PQD system. However, one may ask whether phonons in the other spatial coordinates x and y also have an impact on the process nonetheless. To answer this question the z-coordinate phonons implemented by Eq. (10) are replaced with those in the other coordinates according to Eq. (11). Tab. 2 reveals an anisotropy, namely that isolated vibrations in x and y do not have more than a numerical effects with rendering x- and y-based rates of $\Gamma^{A1}_{1e1p} = 1.71 \cdot 10^{-9}$ meV and $\Gamma^{A1}_{1e1p} = 8.79 \cdot 10^{-10}$ meV, respectively. This finding is

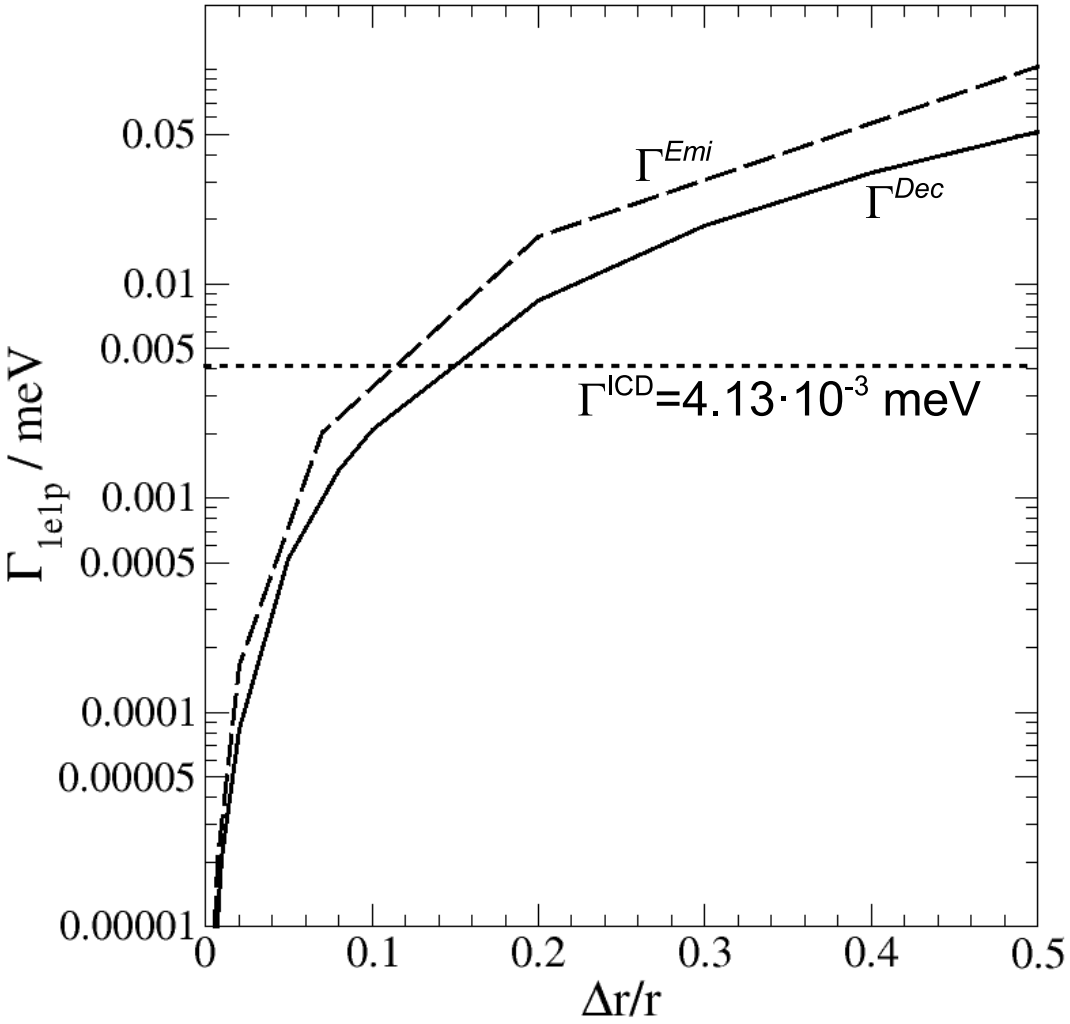

Figure 3. Single-electron single-QD rates Γ_{1e1p} in meV for the dissipation of the A_1 electron in the left QD (straight line, Γ^{A1}_{1e1p}) and for the E_0 electron in the right QD (dashed line, Γ^{E0}_{1e1p}) as function of the relative displacement $\Delta r/r$. The vertical dotted line indicates $\Gamma^{ICD}_{2e2p} = 4.13{\cdot}10^{-3}$ meV.

Table 2. Acoustic phonon A_1 dissipation rate Γ^{A1}_{1p1e} in meV for different individual and combined spatial coordinates 'coord according to equations (10) and (11).

coord	Γ^{A1}_{1p1e}/meV
x	$1.71{\cdot}10^{-9}$
y	$8.79{\cdot}10^{-10}$
z	$8.36{\cdot}10^{-5}$
xy	$3.72{\cdot}10^{-7}$
xz	$8.36{\cdot}10^{-5}$
yz	$8.36{\cdot}10^{-5}$
xyz	$8.36{\cdot}10^{-5}$

Table 3. Acoustic phonon E_0 dissipation rate Γ^{E0}_{1e1p} in meV as function of the displacement parameter $\Delta r/r$.

$\Delta r/r$	Γ^{E0}_{1e1p}/meV
0.001	$4.14{\cdot}10^{-7}$
0.007	$2.03{\cdot}10^{-5}$
0.020	$1.65{\cdot}10^{-4}$
0.070	$2.03{\cdot}10^{-3}$
0.200	$1.65{\cdot}10^{-2}$
0.500	$1.04{\cdot}10^{-1}$
0.500	$8.44{\cdot}10^{-2}$

supported by the fact that all simultaneously applied phonon vibrations in x and z, y and z, and x, y, z direction render a rate identical to Γ^{A1}_{1e1p} of only the z phonon. Only the combined x and y vibration, which would have been expected to give an extremely small rate in the order of 10^{-9} meV, leads to a larger rate of $3.72{\cdot}10^{-7}$ meV, which is only two, rather than four orders of magnitude smaller than Γ^{A1}_{1e1p}. This effect may be due to numerical instabilities in the calculations of very small rates.

Further phase shift effects are tested in making the sinusoidal vibration start with an amplification or a de-amplification of the QD size by changing the sign of the phonon term of Eq. (10). Further a time shift by multiples of $\pi/2$ is introduced by regulating the onset of the vibration by a step function multiplied to the trigonometric functions in Eq. (10) where the sine is exchanged by a negative sine or cosine function with either sign. For all these very early vibration onsets within the first five steps of the propagation, Γ^{A1}_{1e1p} is always the same when evaluated from the time the vibration, and hence the dissipation, actually starts. This was to be expected, because the mechanism of the phonon-mediated dissipation itself is not influenced by the onset time. In reality phonons can of course not be deliberately switched on and off. This calculation is done with view on the relative vibration of both QDs discussed in Sec. 4.3.

To conclude on the A_1 dissipation let me offer a discourse on the mechanistic understanding of the process. Actually one may expect two distinct dissipation channels: one is the transfer of wave function density into the continuum and reflects the general understanding of the acoustic phonon dissipation action. The energy levels are lowered and elevated periodically and the wave packet is never an eigenfunction to them but leaks out of the system. All that leaks out becomes continuum in the Gaussian potential as no other surrounding medium is nearby. Another conceivable dissipation channel is relaxation of the A_1 electron into the A_0 state. Here, excess energy from the QD's electron in the order of the level spacing ΔE_A is dissipated into a matching number of phonon modes with various frequencies. In case of a single-phonon process the energies must match exactly, which they do not in the presented model. In case of a multi-phonon process the energies can be achieved more easily, but the model is not applicable here. And in fact in the present calculations the A_0 state is never populated.

4.1.2. Phonon-Mediated E_0 Dissipation

The right QD has one bound level E_0 and it's electron can dissipate into the continuum (gray arrows on the EQD in Fig. 1). In Fig. 3 the dependence of its dissipation rate

Table 4. Rates Γ in meV of the phonon-mediated A_1, E_0, or the combines A_1E_0 dissipation (upper indices) treated in the two-electron two-QD (lower index $2e2p$), the one-electron two-QD ($1e2p$), and the one-electron one-QD picture ($1e1p$), respectively. Γ^{A1}_{1e2p}, Γ^{E0}_{1e2p}, and $\Gamma^{A1E0}_{2e2p} = \Gamma^{total}_{2e2p} - \Gamma^{ICD}_{2e2p}$ are obtained from electron dynamics calculations, whereas Γ^{A1E0}_{1e1p} and Γ^{A1E0}_{1e2p} are summations of the rates for the corresponding single-electrons processes. The rates listed in the first (second) two lines are for only the AQD (EQD) vibrating. Lines 5-10 belong to phase-shifted vibrations of both dots where the phonon onset times $t_{A,E}$ are given in angular coordinates of the AQD and EQD oscillation.

case	t_A	t_E	Γ^{A1}_{1e2p}/meV	Γ^{E0}_{1e2p}/meV	Γ^{A1E0}_{2e2p}/meV	Γ^{A1E0}_{1e2p}/meV	Γ^{A1E0}_{1e1p}/meV
AQD	0	–	$8.40{\cdot}10^{-5}$	$9.973{\cdot}10^{-7}$	$8.45{\cdot}10^{-5}$	$8.50{\cdot}10^{-5}$	$8.36{\cdot}10^{-5}$
	π	–	$8.40{\cdot}10^{-5}$	$4.179{\cdot}10^{-7}$	$8.44{\cdot}10^{-5}$	$8.44{\cdot}10^{-5}$	$8.36{\cdot}10^{-5}$
EQD	–	0	$4.78{\cdot}10^{-7}$	$1.653{\cdot}10^{-4}$	$1.76{\cdot}10^{-4}$	$1.66{\cdot}10^{-4}$	$1.654{\cdot}10^{-4}$
	–	π	$4.78{\cdot}10^{-7}$	$1.653{\cdot}10^{-4}$	$1.76{\cdot}10^{-4}$	$1.66{\cdot}10^{-4}$	$1.654{\cdot}10^{-4}$
SYN	0	0	$7.28{\cdot}10^{-5}$	$1.664{\cdot}10^{-4}$	$2.50{\cdot}10^{-4}$	$2.39{\cdot}10^{-4}$	$2.49{\cdot}10^{-4}$
	π	π	$7.28{\cdot}10^{-5}$	$1.664{\cdot}10^{-4}$	$2.50{\cdot}10^{-4}$	$2.39{\cdot}10^{-4}$	$2.49{\cdot}10^{-4}$
OFF	0	$\pi/2$	$8.45{\cdot}10^{-5}$	$1.653{\cdot}10^{-4}$	$2.62{\cdot}10^{-4}$	$2.50{\cdot}10^{-4}$	$2.49{\cdot}10^{-4}$
	0	$3\pi/2$	$8.45{\cdot}10^{-5}$	$1.653{\cdot}10^{-4}$	$2.60{\cdot}10^{-4}$	$2.50{\cdot}10^{-4}$	$2.49{\cdot}10^{-4}$
OPP	0	π	$9.61{\cdot}10^{-5}$	$1.642{\cdot}10^{-4}$	$2.67{\cdot}10^{-4}$	$2.60{\cdot}10^{-4}$	$2.49{\cdot}10^{-4}$
	π	0	$9.61{\cdot}10^{-5}$	$1.642{\cdot}10^{-4}$	$2.67{\cdot}10^{-4}$	$2.60{\cdot}10^{-4}$	$2.49{\cdot}10^{-4}$

Γ^{E0}_{1e1p} on the relative displacements is displayed in comparison to Γ^{A1}_{1e1p} and Γ^{ICD}_{2e2p}. Numerical data is given in Tab. 3. Γ^{E0}_{1e1p} increases with increasing displacement in an even stronger way than for the A_1 dissipation. For the unrealistically strong displacement of $\Delta r/r = 0.2$ it is one order of magnitude faster than ICD. For the largest reasonable displacement of 0.02 the rate is $1.65{\cdot}10^{-4}$ meV compared to $\Gamma^{ICD}_{2e2p} = 4.13{\cdot}10^{-3}$ meV and $\Gamma^{A1}_{1e1p} = 8.36{\cdot}10^{-5}$ meV. This shows that although being faster than the A_1 dissipation, the E_0 dissipation alone is still not competitive with ICD.

The phonon vibrations' onset and the vibration direction both do not play a role. The dissipation for z-polarized phonons starts exactly at the onset time with identical rates. Further, differently polarized phonons do only numerically contribute with rates of the order 10^{-11} meV. Therefore, in the remainder of this work the phonons in x and y directions are not any more considered.

4.2. One-Electron Paired Quantum Dot

Due to the boundary conditions of ICD, the paired QDs are largely decoupled from each other [81, 83]. However, in account for the remaining low probability for tunnelling of electrons among the dots and due to the possible longer distance of interactions involving phonons, it is essential to consider the influence of the respective neighbouring QD, may it be still or vibrating, when investigating the phonon dissipation of the A_1 or E_0 electron.

4.2.1. A_1 Dissipation

In the fourth column of Tab. 4 the A_1 electron's dissipation rate Γ^{A1}_{1e2p} is listed for different onset times $t_{A,E}$ of the AQD's and EQD's phonon vibration. In the first two lines are the results for only the AQD vibrating starting at two different times $t_A = 0$ and $t_A = \pi$. The results surprise with the fact that the A_1 dissipation is facilitated solely by the presence of a fixed EQD which enhances the rate by about $1.4{\cdot}10^{-6}$ meV from $8.36{\cdot}10^{-5}$ meV in the one-electron one-QD picture (Tab. 1) to $8.50{\cdot}10^{-5}$ meV. This suggests an additional dissipation pathway in the specific scenario of two nearby, but if at all weakly coupled QDs.

If there was only the AQD solely the here irrelevant $A_1 \rightarrow A_0$ decay and the $A_1 \rightarrow C$ pathway of the electron into the continuum would exist. With an additional E_0 level of a neighbouring EQD, electron tunnelling-mediated dissipation may become possible via $A_1 \rightarrow E_0 \rightarrow A_0$ or $A_1 \rightarrow E_0 \rightarrow C$. To understand the relevance of these pathways, both electron transfer processes are looked at separately over the time of one complete AQD oscillation cycle ($0 < t < 2\pi$) where the AQD becomes according to Eq. (10) first more shallow ($t = \pi/2$) and then deeper ($t = 3\pi/2$) compared to its original shape defined by Eq. (4). Considering the $A_1 \rightarrow E_0$ transition at first one notices that the level spacing $\Delta E(A_1 \rightarrow E_0)$ increases with a more shallow QD and vice versa (Fig. 4(c), solid black line). As a measure for the ease of tunnelling in (d) I consider $\max(|\phi_{A_1}|^2(z_E))$, the maximum value of the reduced density of the A_1 state's wave function in the EQD located at position $z_E = 43.34$ nm. For the considered transition it remains constant with a comparably large value of 0.0014. This means that the $A_1 \rightarrow E_0$ transition is always possible to the same probability.

The second dissipative step $E_0 \rightarrow A_0$ is completing the two-step decay from A_1 into the ground state, but it is competing with $E_0 \rightarrow C$. The energy difference variation $\Delta E(E_0 \rightarrow A_0)$ (Fig.4 (a)) with the AQD oscillation is here slightly larger than the $\Delta E(A_1 \rightarrow E_0)$ variation, because E_{A_0} is more sensitive to geometrical changes than E_{A_1}. At the same time the tunnelling probability $\max(|\phi_{E_0}|^2(z_A))$ (Fig.4 (b)) for the E_0 electron being in the AQD located at position $z_A = -43.34$ nm is one order of magnitude smaller than for the $A_1 \rightarrow E_0$ transition, because the electronic state functions do overlap less. Both effects are in favor for $E_0 \rightarrow C$ and hence allow for the dissipation $A_1 \rightarrow E_0 \rightarrow C$ in addition to $A_1 \rightarrow C$ which is reflected by the higher rate.

By the above findings it became evident that the sheer presence of the EQD influences the electronic processes in the AQD. Hence the logical next step is to investigate the A_1 dissipation when the EQD is not immobile but vibrating. For extracting solely the EQD phonon effect, the AQD is held fixed at first and indeed I find a non-negligible A_1 dissipation rate Γ^{A1}_{1e2p}=4.78·10^{-7} meV. It is in the order of the enhancement of the A_1 phonon dissipation rate discussed in the previous paragraph, when the AQD is vibrating and a fixed EQD is placed nearby. This means opening the channel through E_0 speeds the dissipation by 10^{-7} meV

Again a rationalization via tunnelling pathways can elucidate the way of action of the pure EQD vibration. The left panels of Fig. 4 show in red dashed lines the energy differences and tunnelling measures. When considering the energy spacings, the one for the $A_1 \rightarrow E_0$ partial decay $\Delta E(A_1 \rightarrow E_0)$ (c) decreases when the EQD becomes more shallow, while the one for the $\Delta E(E_0 \rightarrow A_0)$ (a) pathway, increases by about the same amount. The tunnelling measure of the E_0 electron into the A_0 state, $\max(|\phi_{E_0}|^2(z_A))$ (Fig. 4 (b)), again increases with decreasing $\Delta E(E_0 \rightarrow A_1)$ (Fig. 4 (c)) and has small values overall as is intuitive. A significant difference compared to the findings on the AQD variation is found for the $A_1 \rightarrow E_0$ step. $max(|\phi_{A_1}|^2(z_E))$ (Fig. 4 (d)) strongly depends on the EQD variation, whereas it was independent on the AQD variation before. Its maximum value coincides with the minimum of $\Delta E(A_1 \rightarrow E_0)$ and vice versa as is intuitive for tunnelling processes. The average maximum is 0.0014 and equals the value for the AQD vibration. Hence, also upon EQD vibration $A_1 \rightarrow E_0$ is fostered and allows for the $A_1 \rightarrow E_0 \rightarrow C$ process.

The contributions of individual vibrations of either the AQD or the EQD would add up to $\Gamma^{A1}_{1e2p} = 8.45 \cdot 10^{-5}$ meV which is therefore on a first glance the rate to be anticipated in an electron dynamics calculation with both QDs vibrating. But taking into account that phonon-mediated tunnelling between both QDs plays a crucial role

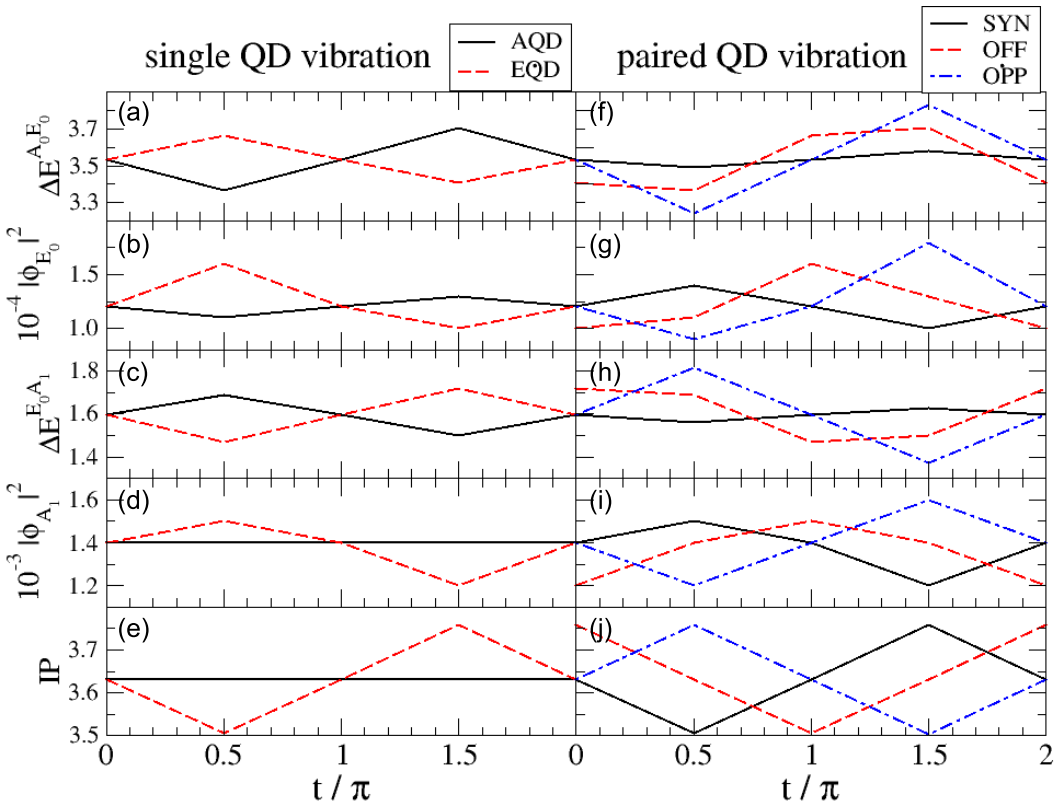

Figure 4. (Color online) Comprehensive energy level differences and probability density changes during one phonon induced binding potential oscillation cycle $0 < t < 2\pi$. The left panels collect single QD vibrations of the AQD (black solid lines) or the EQD (red dashed lines) where the potential becomes shallower at $t = \pi/2$ and deeper at $t = 3\pi/2$. The right panels apply to vibrations of the QD pair according to the SYN (black solid lines), OFF (red dashed lines), or OPP (blue dashed-dotted lines) phase-shift pattern described in the text. Here, the AQD always vibrates as shown in the left panels and the EQD vibration is phase shifted. From top to bottom I show in (a,f) the energy level difference $\Delta E(E_0 \rightarrow A_0)$ in a.u. and in (b,g) the unit-free maximum electron density abbreviated with $\max(|\phi_{E_0}|^2(z_A))$ of the E_0 electron in the AQD at position $z_A = -43.34$ meV. Below the same is displayed for the $A_1 \rightarrow E_0$, that means in (c,h) the energy level difference $\Delta E(A_1 \rightarrow E_0)$ in a.u. and in (d,i) the maximum electron density $max(|\phi_{A_1}|^2(z_E))$ of the A_1 electron density located in the EQD at $z_E = -z_A$. The bottom panels (e,j) display the ionization potential (IP) in meV, which is the energy difference among the first continuum state and the E_0 level.

and moreover strongly depends on the actual level energies during vibration of either of the dots (Fig. 4 (b) and (d)) the total rate must interdependent on the vibration of both dots, i.e. their phase shift indicated by the vibration onset times $t_{A,E}$. Hence different frontier scenarios for the combined vibration of both QDs are established.

SYN: Zero phase shift among the two oscillating binding potentials. Both QDs vibrate synchronously with being most shallow at $t = \pi/2$ and deepest at $t = 3\pi/2$.
OPP: The QDs' vibrations are opposite to each other which implies a phase shift of π starting with a shallowing of the AQD.
OFF: An intermediate phase shift of $\pi/2$ applies, again starting with a shallowing of the AQD.

The summed decay rate of above for either only the AQD or the EQD vibrating is only found in the offset case "OFF" $\Gamma^{A1}_{1e2p}(AQD) + \Gamma^{A1}_{1e2p}(EQD) = \Gamma^{A1}_{1e2p}(OFF)$ (lines 7,8 in Tab. 4. Otherwise the rate is either diminished or enhanced by $1.16{\cdot}10^{-5}$ meV when the two QDs oscillate synchronously (SYN) or opposite (OPP).

For an understanding of this effect the energy differences and tunneling probabilities for a full oscillation cycle of both QDs are visualized (Fig. 4, right panels). In the graph the AQD shallows first and the EQD vibrates according the different pattern. Comparing the left column for only one QD vibrating it becomes immediately apparent that the effects of both dots vibrating span a wider range in all investigated quantities. For the SYN case (black, solid line) the four measures of above (f) $\Delta E(E_0 \rightarrow A_0)$, (g) $max(|\phi_{E_0}|^2(z_A))$, (h) $\Delta E(A_1 \rightarrow E_0)$, and (i) $max(|\phi_{A_1}|^2(z_E))$ span the overall smallest range, which can be there considered as the major reason for the likewise smallest decay rate. Both relevant energy differences, $\Delta E(E_0 \rightarrow A_0)$ (Fig. 4 (f)) and $\Delta E(A_1 \rightarrow E_0)$ (Fig. 4 (h)), remain relatively constant when both QDs simultaneously become smaller at $t = \pi/2$. These small ΔE correspond to the largest tunnelling measures $max(|\phi_{E_0}|^2(z_A))$ (g) and $max(|\phi_{A_1}|^2(z_E))$ (i).

For the OFF (magenta, dashed line) and the OPP (blue, dashed-double dotted line) cases the pathway $A_1 \rightarrow E_0 \rightarrow A_0$ is completely open at $t = \pi$ and $t = 3\pi/2$, respectively, with increasing tunnelling probability. The respective maximal values $max(|\phi_{E_0}|^2(z_A))$ and $max(|\phi_{A_1}|^2(z_E))$ are 0.00018 and 0.0016 in the OFF case, 0.00016 and 0.0015 in the OPP case, and 0.00014 and 0.0015 in the SYN case. Contrary, their minima are almost identical with being slightly larger in the OFF case among all three phase-shift cases. Note, however, that in all cases $max(|\phi_{E_0}|^2(z_A)) << max(|\phi_{A_1}|^2(z_E))$ which means that any dissipation into A_0 is less likely than dissipation into the continuum.

4.2.2. E_0 Dissipation

The emission of the E_0 electron into the continuum is the other partial process of ICD and itself affected by the phonons. Tab. 4 comprises the respective rates Γ^{E0}_{1e2p} in its fifth column. The most crucial scenario of a sole EQD vibration at two different onset times t_E (lines 3,4) shows that already the presence of an fixed AQD induces a rate decrease by $1{\cdot}10^{-7}$ from $\Gamma^{A1E0}_{1e1p} = 1.654 \cdot 10^{-4}$ (last column) to $\Gamma^{E0}_{1e2p}(EQD) = 1.653 \cdot 10^{-4}$ (fifth column). Instead of direct electron emission from the level E_0, the electron can now alternatively tunnel into the levels of the neighbouring AQD for which the measure $\max(|\phi_{E_0}|^2(z_A))$ (Fig. 4 (b)) is depending on the EQDs oscillation. The larger the probability to find the E_0 electron in the AQD the smaller the ionization potential (Fig. 4 (e)).

Interestingly, also if only the AQD is vibrating the emission rate is still non-negligible

which is caused by the additional emission pathway $E_0 \rightarrow A_1 \rightarrow C$. Reproducibly, numerically different rates $\Gamma^{E0}(AQD) = 9.973 \cdot 10^{-7}$ and $4.179 \cdot 10^{-7}$ meV have been obtained at the different onset times $t = 0$ and $t = \pi$. As both these rates are very small, summing them with Γ^{E0}_{1e2p} for only the EQD vibrating renders similar values $1.663{\cdot}10^{-4}$ and $1.657{\cdot}10^{-4}$ meV, respectively.

These numbers are most closely reproduced in the SYN case of the simultaneous vibration of both QDs (lines 5,6 of Tab. 4) which means that the E_0 emission profits from a simultaneous in- or decrease of all electronic levels and particularly from overall low tunnelling effects (Fig. 4(b,d), black solid lines).

In contrast to that an offset of $\pi/2$ (OFF) leads to a decrease of the rate by $1.123{\cdot}10^{-6}$ meV and a more pronounced offset during opposite vibrations (OPP) to a further decrease by $1.102{\cdot}10^{-6}$ meV. This effect is inverse to what was encountered during A_1 dissipation and moreover internal rate differences are one order of magnitude smaller. As on the other hand the E_0 dissipation rate itself is one order of magnitude larger than the A_1 rate, the conclusion is that the emission is not very sensitive to changes in the phonon vibration pattern.

4.3. Two-Electron Double Quantum Dot

4.3.1. Inter-Coulombic Decay

The key question in this work is to what degree phonons (all gray arrows in Fig. 1) are competitive to the ICD (black arrows) of the A_1E_0 resonance state in a PQD. In the previous sections it was shown that the individual A_1 and E_0 dissipation rates for both the one- or two-vibrating potential case are in the order of $\Gamma^{A1} \approx 10^{-5}$ meV and $\Gamma^{E0} \approx 10^{-4}$ meV, respectively and hence smaller then the unaffected ICD rate Γ^{ICD}_{2e2p} $= 4.1310^{-3}$ meV [81]. Therefore the expectation is that ICD will still be found to be competitive in a full-dynamics calculation including both electrons and the vibration of both QDs. Indeed all total rates of this work are on average $\Gamma^{total}_{2e2p} \approx 4.4 \cdot 10^{-3}$ meV and with that higher than Γ^{ICD}_{2e2p} by the amount suggested by the phonons.

A graphical representation of the regular exponential decay of $|a(t)|^2$ of the ICD process is found in Fig. 5 (black-solid line, panel (a)) together with graphs of combined ICD and phonon processes. From these graphs, especially from zooming into the picture, it becomes evident how the ICD rate Γ^{ICD}_{2e2p} is affected by phonon dissipations Γ^{A1E0}_{2e2p} in all cases. The squared autocorrelation loss, however, is dominated by ICD throughout. The most significant speedup of the $|a(t)|^2$ decay comes from the E_0 dissipation (inset (b), grey solid line) followed by the A_1 dissipation (inset (b), brown solid line). Finally, the differences of $|a(t)|^2$ by both QDs vibrating are approximately as large as the two individual contributions in the ordering of SYN (black dashed line) decaying slowest followed by OFF (brown dashed line) and OPP (gray dashed line) as highlighted in inset (c).

Numerical two-electron two-potential dissipation rates Γ^{A1E0}_{2e2p} are listed in the sixth column of Tab. 4. They were obtained as $\Gamma^{A1E0}_{2e2p} = \Gamma^{total}_{2e2p} - \Gamma^{ICD}_{2e2p}$ where Γ^{total}_{2e2p} was determined from the exponential decay of the autocorrelation function for the full two electron dynamics including phonons (cf. Fig. 5) and Γ^{ICD}_{2e2p} excluding phonons. The values reveal quantitative numbers for phonon effects of the combined A_1 and E_0 dissipation processes and further correlation effects among electrons and phonons in all combinations.

From the rates of single-QD vibrations in lines 1-4 of Tab. 4 it becomes again

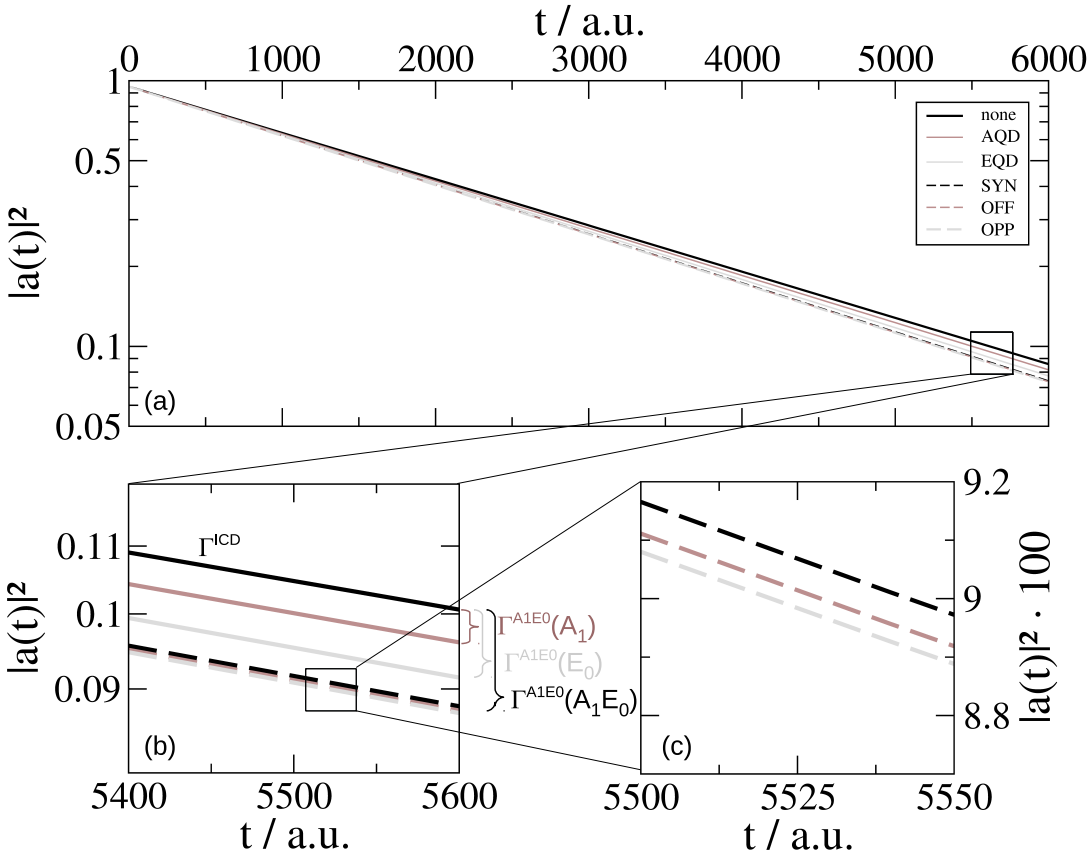

Figure 5. (Color online) (a) Absolute squared of the autocorrelation function $|a(t)|^2$ is shown for the pure, phonon-free ICD (black, solid line), giving Γ^{ICD}_{2e2p}, and for the different phonon dissipations Γ^{A1E0}_{2e2p} ranging from the vibration of the AQD or EQD only (brown and gray solid lines, (b)) to that of both QDs in different combinations (c), namely SYN, OFF, and OPP (black, brown, and grey dashed lines).

apparent that the contribution of the AQD's vibration is with $8.44{\cdot}10^{-5}$ meV in the full dynamics calculations roughly half as significant as the one of the EQD with $1.76{\cdot}10^{-4}$ meV. Cross-connecting to Γ^{A1}_{1e2p} and Γ^{E0}_{1e2p} of the one-electron two-QD picture, shows consistently that Γ^{A1E0}_{2e2p} is dominated by Γ^{A1}_{1e2p} when only the AQD is vibrating (lines 1,2) and by Γ^{E0}_{1e2p} when only the EQD is vibrating (lines 3,4).

When both phonon vibrations and both electrons are considered at a time, correlation effects among two electrons, two phonons, or electrons and phonons come into play. To evaluate them two further columns were added to Tab. 4 that belong to single-electron calculations combined for both processes. In column seven there are rates Γ^{A1E0}_{1e2p} based on the one-electron two-QD system discussed in Sec. 4.2.1. $\Gamma^{A1E0}_{1e1p} = \Gamma^{A1}_{1e1p} + \Gamma^{E0}_{1e1p}$ are based on rates from Tab. 4 and the discussion in Sec. 4.1 and belong to the one-electron one-QD picture.

The comparison of the two- and single-electron phonon dissipation rates Γ^{A1E0}_{2e2p} and Γ^{A1E0}_{1e2p} reveals that the lower-complexity case of non-interacting electrons leads to a systematic underestimation of the rate by about $1{\cdot}10^{-5}$ meV. The energy contribution can clearly be assigned to the electron-electron correlation and exchange energy. When additionally removing one of the QDs (last column of Tab. 4), the value is again smaller by about $1{\cdot}10^{-6}$ meV. This is caused by two effects. Firstly, the tunnelling pathway for dissipation through the neighbouring QD is closed, which was determined previously to change the rate by $5{\cdot}10^{-8}$ meV. Secondly, rates do not contain the crosswise electron-phonon interaction energy, where crosswise means the interaction of the AQD phonon and the E_0 electron and vice versa.

In the overlaid vibration of both QDs the emission rate Γ^{E0}_{2e2p} dominates the order of magnitude of Γ^{A1E0}_{2e2p} as it is in the order of 10^{-4} meV and twice as large as Γ^{A1}_{2e2p}. Γ^{A1}_{2e2p} instead has a one order of magnitude stronger dependence on the offset than Γ^{E0}_{2e2p} which was found to be $1 \cdot 10^{-5}$ meV. Hence, the trend for the offset scenarios is the same for Γ^{A1E0}_{2p2e} and for Γ^{A1}_{2p2e}, namely the rate is highest for opposite phonon vibrations (OPP) and lowest for synchronous vibrations (SYN). The same findings are true for the combined decay and emission rates Γ^{A1E0}_{1e2p} in the one-electron two-QD scenario.

The ultimate reduction of complexity reveals that the phonon rate Γ^{E1A0}_{1e1p} with only one vibrating potential is in all cases identical to the sum of emission and decay rate. The offset has no impact here, because in the one-electron one-QD picture the phonon-phonon correlation is neglected. It can be estimated to be in the order of 10^{-5} meV which is the variation of Γ^{A1E0}_{1e2p} (differing only by the including phonon-phonon interaction) with different offsets. As the values Γ^{A1E0}_{1e1p} and Γ^{A1E0}_{1e2p} are on average identical the estimate for the electron-electron correlation contribution of $1 \cdot 10^{-5}$ meV from the previous paragraph is confirmed.

So finally rate contributions are $1 \cdot 10^{-5}$ meV for the phonon-phonon, $1 \cdot 10^{-6}$ meV for the crosswise electron-phonon, and $1 \cdot 10^{-5}$ meV for the electron-electron interaction. AQD and EQD phonons contribute by $1 \cdot 10^{-5}$ meV and $1 \cdot 10^{-4}$ meV which are basically the values for the local electron-phonon interaction. All theses interconnected processes are much less important than ICD itself.

5. Discussion

In this study the explicit treatment of phonons is exclusive for acoustic phonons by implementing a time-dependent binding potential. Optical phonons are argued to be less relevant due to the energetic mismatch of their energies with the level spacings. Anyway, in order to properly implement optical phonons into the model, one would have to account for the fact that optical phonons mechanistically induce a dipole moment which then couples to the electronic states through Fröhlich interaction. Such dipole-dipole coupling in a two-level system should thus enter the Hamiltonian matrix in an off-diagonal matrix element as

$$\begin{pmatrix} 0 & V^{OP}(t) \\ V^{OP}(t) & 0 \end{pmatrix} \begin{pmatrix} |A_0\rangle \\ |A_1\rangle \end{pmatrix} \tag{14}$$

as encountered for the state transitions induced by an oscillating laser field, e.g.

$$V^{OP} = -\mu\varepsilon_0 \cos(\omega_{OP} t) \tag{15}$$

with the frequency ω_{OP} and the transition dipole moment μ among the two states [69, 82]. If the equation was implemented, the choice of field strengths ε_0 would be a sensitive quantity for which no reference is known. Hence, I leave such investigation for a future study.

Here I only give a further hint on the relevance of optical phonons by using the acoustic phonon implementation (Eq. (10)) with the longitudinal optical phonon frequency for GaAs of 36 meV [94, 95] and $\Delta r/r = 0.02$. Doing so for the two-electron two-QD system renders an expectedly low dissipation rate of Γ^{opt}_{2e2p} which is three orders of magnitude lower than the ICD rate itself and one order lower than acoustic phonon dissipation rate .

Finally, the acoustic phonon dissipation time is 2.5 ns compares to the non-phonon ICD time τ =159 ps as did the rates. It is roughly half of the spontaneous radiative decay time of 5.7 ns found for the PQD system earlier [80].

6. Conclusion

Established two-electron dynamics calculations on the inter-Coulombic decay (ICD) process in two binding potentials reflecting quantum dots (QDs) have been extended by a treatment for acoustic phonons. Such phonons were understood to be a possible competitor process in dissipating excited states on the same time scale as ICD itself. In nanomaterials acoustic vibrations lead to macroscopic effects as e. g. to QD breathing modes. Hence, in a frozen-phonon approach the QD binding potentials were straightforwardly varied in size harmonically in all directions. Dissipation in the sense of electron emission from either QD was observed and one (two) orders of magnitude slower than ICD for the emitter (acceptor) QD vibration. From a gradual increase of complexity through adding phonon and electron terms successively, several individual contributions from different interactions were deduced.

Acknowledgements

In 2011 Nimrod Moiseyev and I published both our first paper on QD-ICD with different models and methodologies. I am grateful for our discussions in that time in which I learned more from Nimrod's different viewing angle. Another view has significantly been inspired by the curiosity of the scientific community on the role of phonons in QD-ICD. Several people deserve thank for helping me answering this question. Particularly, I would like to thank Ioan Baldea for introducing me to theories of phonons in nanomaterials, Andreas Komnik, who sketched the applied phonon description, Fabian Langkabel for typesetting the manuscript as well as the internship students Lena Steuer, Maik Rudolff, and Joana-Lysiane Schäfer, who performed first test calculations.

Funding

The work was supported by the Deutsche Forschungsgemeinschaft under Grant 3770/2-1; the Volkswagen foundation under the Freigeist fellowship 89525.

Disclosure statement

There is not conflict of interest.

References

[1] G.E. Jellison, Jr. and F.A. Modine, Phys. Rev. B **27**, 7466 (1983).
[2] P. Lautenschlager, M. Garriga, L. Viña and M. Cardona, Phys. Rev. B **36**, 4821 (1987).
[3] A. Marini, Phys. Rev. Lett. **101**, 106405 (2008).
[4] S. Logothetidis, J. Petalas, H.M. Polatoglou and D. Fuchs, Phys. Rev. B **46**, 4483 (1992).
[5] A. Eiguren, C. Ambrosch-Draxl and P.M. Echenique, Phys. Rev. B **79**, 245103 (2009).
[6] F. Giustino, S.G. Louie and M.L. Cohen, Phys. Rev. Lett. **105**, 265501 (2010).
[7] S. Poncé, G. Antonius, Y. Gillet, P. Boulanger, J. Laflamme Janssen, A. Marini, M. Côté and X. Gonze, Phys. Rev. B **90**, 214304 (2014).
[8] M. Bernardi, J. Mustafa, J.B. Neaton and S.G. Louie, Nat. Commun. **6**, 7044 (2015).
[9] M. Bernardi, D. Vigil-Fowler, J. Lischner, J.B. Neaton and S.G. Louie, Phys. Rev. Lett. **112**, 257402 (2014).
[10] M. Bernardi, D. Vigil-Fowler, C.S. Ong, J.B. Neaton and S.G. Louie, Proc. Natl. Acad. Sci. USA **112**, 5291 (2015).
[11] F. Caruso and F. Giustino, Phys. Rev. B **94**, 115208 (2016).
[12] M. Glässl, A.M. Barth and V.M. Axt, Phys. Rev. Lett. **110**, 147401 (2013).
[13] A.J. Ramsay, T.M. Godden, S.J. Boyle, E.M. Gauger, A. Nazir, B.W. Lovett, A.M. Fox and M.S. Skolnick, Phys. Rev. Lett. **105**, 177402 (2010).
[14] R. Ferreira and G. Bastard, Phys. Rev. B **40**, 1074 (1989).
[15] R. Ferreira, B. Soucail, P. Voisin and G. Bastard, Phys. Rev. B **42**, 11404 (1990).
[16] H. Benisty, C.M. Sotomayor-Torres and C. Weisbuch, Phys. Rev. B **44**, 10945 (1991).
[17] H. Benisty, Phys. Rev. B **51**, 13281 (1995).
[18] A. Zrenner, J. Chem. Phys. **112**, 7790 (2000).
[19] R.R. Cooney, S.L. Sewall, E.A. Dias, D.M. Sagar, K.E.H. Anderson and P. Kambhampati, Phys. Rev. B **75**, 245311 (2007).

[20] T. Fujisawa, T.H. Oosterkamp, W.G. van der Wiel, B.W. Broer, R. Aguado, S. Tarucha and L.P. Kouwenhoven, Science **282**, 932 (1998).
[21] T. Brandes and B. Kramer, Phys. Rev. Lett. **83**, 3021 (1999).
[22] I. Magnusdottir, A.V. Uskov, S. Bischoff, B. Tromborg and J. Mørk, J. Appl. Phys. **92**, 5982 (2002).
[23] M. Glanemann, V.M. Axt and T. Kuhn, Phys. Rev. B **72**, 045354 (2005).
[24] S. Trumm, M. Wesseli, H.J. Krenner, D. Schuh, M. Bichler, J.J. Finley and M. Betz, Appl. Phys. Lett. **87**, 153113 (2005).
[25] R. Ferreira and G. Bastard, Nanoscale Res Lett **1**, 120 (2006).
[26] S. Kvaal, Phys. Rev. A **84**, 022512 (2011).
[27] F. Jiang, J. Jin, S. Wang and Y.J. Yan, Phys. Rev. B **85**, 245427 (2012).
[28] M. Grundmann, Physica E **5**, 167 (2000).
[29] N.N. Ledentsov, Semicond. Sci. Technol. **26**, 014001 (2011).
[30] J.M. Caruge, J.E. Halpert, V. Wood, V. Bulović and M.G. Bawendi, Nat. Photonics **2**, 247 (2008).
[31] L. Zhuang, L. Guo and S.Y. Chou, Appl. Phys. Lett. **72**, 1205 (1998).
[32] S. Maimon, E. Finkman, G. Bahir, S.E. Schacham, J.M. Garcia and P.M. Petroff, Appl. Phys. Lett. **73**, 2003 (1998).
[33] A.J. Nozik, M.C. Beard, J.M. Luther, M. Law, R.J. Ellingson and J.C. Johnson, Chem. Rev. **110**, 6873 (2010).
[34] J. Shen, Y. Zhu, X. Yang and C. Li, Chem. Commun. **48**, 3686 (2012).
[35] S. Buller and J. Strunk, J. Energy Chem. **25**, 171 (2016).
[36] D. Loss and D.P. DiVincenzo, Phys. Rev. A **57**, 120 (1998).
[37] T.H. Stievater, X. Li, D.G. Steel, D. Gammon, D.S. Katzer, D. Park, C. Piermarocchi and L.J. Sham, Phys. Rev. Lett. **87**, 133603 (2001).
[38] W. Luo, J. Lai, D. Lu, C. Du, Y. Liu, S. Gong, D. Shi and C. Guo, J. Phys. B: At. Mol. Opt. Phys. **45**, 035402 (2012).
[39] M. Sugawara, K. Mukai and H. Shoji, Appl. Phys. Lett. **71**, 2791 (1997).
[40] P. Han and G. Bester, Phys. Rev. B **92**, 125438 (2015).
[41] S.M. Reimann and M. Manninen, Rev. Mod. Phys. **74**, 1283 (2002).
[42] M.A. Cusack, P.R. Briddon and M. Jaros, Phys. Rev. B **54**, R2300 (1996).
[43] M.V. Rama Krishna and R.A. Friesner, Phys. Rev. Lett. **67**, 629 (1991).
[44] L.W. Wang, J. Kim and A. Zunger, Phys. Rev. B **59**, 5678 (1999).
[45] A. Puzder, A.J. Williamson, F. Gygi and G. Galli, Phys. Rev. Lett. **92**, 217401 (2004).
[46] A. Franceschetti and A. Zunger, Phys. Rev. Lett. **78**, 915 (1997).
[47] A. Zunger, MRS Bulletin **23**, 35 (1998).
[48] J.R. Cárdenas and G. Bester, Phys. Rev. B **86**, 115332 (2012).
[49] G. Hermann and J.C. Tremblay, J. Phys. Chem. C **119**, 25606 (2015).
[50] G. Bastard, *Wave Mechanics Applied to Semiconductor Heterostructures* (, , 1992).
[51] M. Rontani, C. Cavazzoni, D. Bellucci and G. Goldoni, J. Chem. Phys. **124**, 124102 (2006).
[52] Y. Sajeev and N. Moiseyev, Phys. Rev. B **78**, 075316 (2008).
[53] H. Tamura, J.M. Mallet, M. Oheim and I. Burghardt, J. Phys. Chem. C **113**, 7548 (2009).
[54] U. Woggon, *Optical Properties of Semiconductor Quantum Dots* (, , 1997).
[55] P.E. Lippens and M. Lannoo, Phys. Rev. B **39**, 10935 (1989).
[56] P.E. Lippens and M. Lannoo, Phys. Rev. B **41**, 6079 (1990).
[57] G.T. Einevoll, Phys. Rev. B **45**, 3410 (1992).
[58] L.M. Ramaniah and S.V. Nair, Phys. Rev. B **47**, 7132 (1993).
[59] T. Takagahara, Phys. Rev. Lett. **71**, 3577 (1993).
[60] R. Charrour, M. Bouhassoune, M. Barnoussi and M. Fliyou, Phys. Stat. Sol. (b) **219**, 287 (2000).
[61] P. Saalfrank, Chem. Rev. **106**, 4116 (2006).
[62] A. Vagov, M.D. Croitoru, M. Glässl, V.M. Axt and T. Kuhn, Phys. Rev. B **83**, 094303

(2011).
[63] S. Maier, T.L. Schmidt and A. Komnik, Phys. Rev. B **83**, 085401 (2011).
[64] U. Bockelmann and G. Bastard, Phys. Rev. B **42**, 8947 (1990).
[65] S.Y. Savrasov, D.Y. Savrasov and O.K. Andersen, Phys. Rev. Lett. **72**, 372 (1994).
[66] W. Frank, C. Elsässer and M. Fähnle, Phys. Rev. Lett. **74**, 1791 (1995).
[67] M.M. Dacorogna, M.L. Cohen and P.K. Lam, Phys. Rev. Lett. **55**, 837 (1985).
[68] P. Han and G. Bester, Phys. Rev. B **85**, 235422 (2012).
[69] A. Bande, J. Chem. Phys. **138**, 214104 (2013).
[70] L.S. Cederbaum, J. Zobeley and F. Tarantelli, Phys. Rev. Lett. **79** (24), 4778 (1997).
[71] U. Hergenhahn, J. Electron Spectrosc. Relat. Phenom. **184**, 78 (2011).
[72] T. Jahnke, J. Phys. B: At. Mol. Opt. Phys. **48**, 082001 (2015).
[73] S.D. Stoychev, A.I. Kuleff and L.S. Cederbaum, J. Am. Chem. Soc. **133**, 6817 (2011).
[74] P.H.P. Harbach, M. Schneider, S. Faraji and A. Dreuw, J. Phys. Chem. Lett. **4**, 943 (2013).
[75] K. Gokhberg, P. Kolorenč, A.I. Kuleff and L.S. Cederbaum, Nature **505**, 661 (2014).
[76] E. Alizadeh, T.M. Orlando and L. Sanche, Annu. Rev. Phys. Chem. **66**, 379 (2015).
[77] I. Cherkes and N. Moiseyev, Phys. Rev. B **83**, 113303 (2011).
[78] T. Goldzak, L. Gantz, I. Gilary, G. Bahir and N. Moiseyev, Phys. Rev. B **91**, 165312 (2015).
[79] T. Goldzak, L. Gantz, I. Gilary, G. Bahir and N. Moiseyev, Phys. Rev. B **93**, 045310 (2016).
[80] A. Bande, K. Gokhberg and L.S. Cederbaum, J. Chem. Phys. **135**, 144112 (2011).
[81] P. Dolbundalchok, D. Peláez, E. Aziz and A. Bande, J. Comput. Chem. **37**, 2249 – 2259 (2016).
[82] A. Haller, Y.C. Chiang, M. Menger, E.F. Aziz and A. Bande, Chem. Phys. **482**, 135 (2017).
[83] F. Weber, E.F. Aziz and A. Bande, J. Coput. Chem. **38**, 2141 (2017).
[84] A. Haller and A. Bande, in print at J. Chem. Phys. (2018).
[85] H.D. Meyer, U. Manthe and L.S. Cederbaum, Chem. Phys. Lett. **165**, 73 (1990).
[86] U. Manthe, H.D. Meyer and L.S. Cederbaum, J. Chem. Phys. **97**, 3199 (1992).
[87] P. Kolorenč and N. Sisourat, J. Chem. Phys. **143**, 224310 (2015).
[88] R. Santra and L.S. Cederbaum, Phys. Rep. **368** (1), 1 (2002).
[89] V. Averbukh, P. Kolorenč, K. Gokhberg and S. Cederbaum, in (Springer, Netherlands, 2009), *Advances in the Theory of Atomic and Molecular Systems*, Vol. 20, p. 155.
[90] K. Kreidi, P.V. Demekhin, T. Jahnke, T. Weber, T. Havermeier, X. Liu, Y. Morishita, S. Schössler, L. Schmidt, M. Schöffler, M. Odenweller, N. Neumann, L. Foucar, J. Titze, B. Ulrich, F. Sturm, C. Stuck, R. Wallauer, S. Voss, I. Lauter, H.K. Kim, M. Rudloff, H. Fukuzawa, G. Prümper, N. Saito, K. Ueda, A. Czasch, O. Jagutzki, H. Schmidt-Böcking, S. Scheit, L.S. Cederbaum and R. Dörner, Phys. Rev. Lett. **103** (3), 033001 (2009).
[91] N. Sisourat, N.V. Kryzhevoi, P. Kolorenč, S. Scheit and L.S. Cederbaum, Phys. Rev. A **82**, 053401 (2010).
[92] N. Sisourat, N.V. Kryzhevoi, P. Kolorenč, S. Scheit, T. Jahnke and L.S. Cederbaum, Nat. Phys. **6**, 508 (2010).
[93] Y.C. Chiang, F. Otto, H.D. Meyer and L.S. Cederbaum, Phys. Rev. Lett. **107**, 173001 (2011).
[94] New Semiconductor Materials. Biology Systems. ¡http://www.ioffe.ru/SVA/NSM/Semicond/GaAs/¿ (accessed April 15, 2016).
[95] J.L.T. Waugh and G. Dolling, Phys. Rev. **132**, 2410 (1963).
[96] E.A. Zibik, T. Grange, B.A. Carpenter, N.E. Porter, R. Ferreira, G. Bastard, D. Stehr, S. Winnerl, M. Helm, H.Y. Liu, M.S. Skolnick and L.R. Wilson, Nat. Mater. **8**, 803 (2009).
[97] M. Uiberacker, T. Uphues, M. Schultze, A.J. Verhoef, V. Yakovlev, M.F. Kling, J. Rauschenberger, N.M. Kabachnik, H. Schröder, M. Lezius, K.L. Kompa, H.G. Muller, M.J.J. Vrakking, S. Hendel, U. Kleineberg, U. Heinzmann, M. Drescher and F. Krausz,

Nature **446**, 627 (2007).
[98] J. Singh, *Physics of Semiconductors and Their Heterostructures* (, , 1993).
[99] K. Keren, A. Stern and U. Sivan, Eur. Phys. J. B **18**, 311 (2000).
[100] A.L. Efros, M. Rosen, M. Kuno, M. Nirmal, D.J. Norris and M. Bawendi, Phys. Rev. B **54**, 4843 (1996).
[101] V. Shikin, S. Nazin, D. Heitmann and T. Demel, Phys. Rev. B **43**, 11903 (1991).
[102] L. Jacak, P. Hawrylak and A. Wójs, *Quantum Dots* (Springer-Verlag, Berlin, Heidelberg, 1998).
[103] Y. Kayanuma and H. Momiji, Phys. Rev. B **41**, 10261 (1990).
[104] A. Bande, F.M. Pont, P. Dolbundalchok, K. Gokhberg and L.S. Cederbaum, EPJ Web Conf. **41**, 04031 (2013).
[105] W.G. Spitzer, J. Appl. Phys. **34**, 792 (1963).
[106] H.D. Meyer, F. Gatti and G.A. Worth, editors, *Multidimensional Quantum Dynamics* (WILEY-VCH, Weinheim, 2009).
[107] M.H. Beck, A. Jäckle, G.A. Worth and H.D. Meyer, Phys. Rep. **324**, 1 (2000).
[108] A. Jäckle and H.D. Meyer, J. Chem. Phys. **104**, 7974 (1996).
[109] A. Jäckle and H.D. Meyer, J. Chem. Phys. **109**, 3772 (1998).
[110] K. Parlinski, Z.Q. Li and Y. Kawazoe, Phys. Rev. Lett. **78**, 4063 (1997).
[111] S. Grieshammer, T. Zacherle and M. Martin, Phys. Chem. Chem. Phys. **15**, 15935 (2013).